

RESEARCH PAPER

Genetically clustered antifungal phytocytokines and receptor protein family members cooperate to trigger plant immune signaling

Julie Lintz^{1, ID}, Yukihisa Goto^{2, ID}, Kyle W. Bender^{2, ID}, Raphaël Bchini^{1, ID}, Guillaume Dubrulle^{1, ID}, Euan Cawston^{1, ID}, Cyril Zipfel^{2,3, ID}, Sébastien Duplessis^{1, ID}, and Benjamin Petre^{1*, ID}

¹ Université de Lorraine, INRAE, IAM, Nancy, F-54000, France

² Institute of Plant and Microbial Biology, Zurich-Basel Plant Science Center, University of Zurich, 8008 Zurich, Switzerland

³ The Sainsbury Laboratory, University of East Anglia, Norwich Research Park, Norwich NR4 7UH, UK

* Correspondence: benjamin.petre@univ-lorraine.fr

Received 20 February 2024; Editorial decision 2 July 2024; Accepted 8 July 2024

Editor: Monica Höfte, University of Ghent, Belgium

Abstract

Phytocytokines regulate plant immunity by cooperating with cell surface proteins. *Populus trichocarpa* RUST INDUCED SECRETED PEPTIDE 1 (PtRISP1) exhibits an elicitor activity in poplar, as well as a direct antimicrobial activity against rust fungi. The PtRISP1 gene directly clusters with a gene encoding a leucine-rich repeat receptor protein (LRR-RP), that we termed RISP-ASSOCIATED LRR-RP (PtRALR). In this study, we used phylogenomics to characterize the RISP and RALR gene families, and molecular physiology assays to functionally characterize RISP/RALR pairs. Both RISP and RALR gene families specifically evolved in Salicaceae species (poplar and willow), and systematically cluster in the genomes. Despite a low sequence identity, *Salix purpurea* RISP1 (SpRISP1) shows properties and activities similar to PtRISP1. Both PtRISP1 and SpRISP1 induced a reactive oxygen species (ROS) burst and phosphorylation of mitogen-activated protein kinases (MAPKs) in *Nicotiana benthamiana* leaves expressing the respective clustered RALR. PtRISP1 also triggers a rapid stomatal closure in poplar. Altogether, these results indicate that plants evolved phytocytokines with direct antimicrobial activities, and that the genes encoding these phytocytokines co-evolved and physically cluster with genes encoding LRR-RPs required to initiate immune signaling.

Keywords: Antimicrobial peptide, bifunctional peptide, elicitor peptide, pattern recognition receptor (PRR), pattern-triggered immunity (PTI), plant immunity, *Pucciniales*, woody plant.

Introduction

The plant immune system fends off pathogens and prevents diseases (Ngou *et al.*, 2022). This system notably uses defense peptides commonly exhibiting either an antimicrobial activity or an immunomodulatory activity (Tavormina *et al.*, 2015). Antimicrobial peptides (AMPs) possess a cytotoxic activity

that directly targets microbes (Bakare *et al.*, 2022), whereas immunomodulatory peptides (also called phytocytokines analogous to metazoan cytokines) modulate cell immune signaling via the activation of specific cell surface proteins (Yamaguchi and Huffaker, 2011; Hou *et al.*, 2021; Rhodes *et al.*, 2021;

Rzemieniewski and Stegmann, 2022). In animals, some defense peptides are bi-functional—they exhibit both antimicrobial and immunomodulatory activities. These peptides are referred to as host defense peptides (HDPs), and emerge as molecules with high valorization potential, as their many activities can be exploited for therapeutic purposes (Yeung et al., 2011; Hilchie et al., 2013; Haney et al., 2019; Sun et al., 2023). In plants, only a handful of HDP candidates have been described, and the concept of defense peptides having two distinct roles within the immune system has only recently emerged (Petre, 2020).

Plant cell surface proteins reside at the plasma membrane and notably involve members of the so-called receptor kinase (RK) or receptor protein (RP) gene families (DeFalco and Zipfel, 2021). Members of those families with extracellular leucine-rich repeat (LRR) domains are referred to as LRR-RKs or LRR-RPs, and are activated by specific peptides or proteins to initiate immune signaling events via the activation of intracellular kinases (Ngou et al., 2022). Unlike LRR-RKs, LRR-RPs lack a cytosolic kinase domain and require the universal adaptor kinase SUPPRESSOR OF BIR11 (SOBIR1) to accumulate and initiate immune signaling (Liebrand et al., 2013; Bi et al., 2016; Gust et al., 2017; Ranf, 2017). LRR-RP or LRR-RK activation rapidly triggers a set of downstream responses, notably the transient accumulation of reactive oxygen species (ROS) and the activation by phosphorylation of mitogen-activated protein kinases (MAPKs) (Gust and Felix, 2014). Among the 19 known LRR-RPs involved in immune signaling activation, only the INCEPTIN RECEPTOR (INR) is activated by a plant peptide (Snoeck et al., 2023).

The *Salicaceae* family of plants regroups two main genera: *Populus* (poplar trees) and *Salix* (willow trees). The black cottonwood *Populus trichocarpa* was the first tree to have its genome sequenced and made available to the scientific community (Tuskan et al., 2006). Poplar is a model perennial plant widely used to study growth- and immunity-related processes (Bradshaw et al., 2000; Jansson and Douglas, 2007; Duplessis et al., 2009; Hacquard et al., 2011). Investigations of the poplar immune system revealed striking differences compared with annual plants, notably in terms of immune receptor content and diversity, phytohormonal regulation, and defense peptide diversity (Kohler et al., 2008; Hacquard et al., 2011; Ullah et al., 2022). Poplar or willow LRR-RPs have not been functionally investigated so far.

In 2007, a transcriptomic analysis of poplar leaves revealed an orphan gene called *RUST INDUCED SECRETED PEPTIDE* (*RISP*, hereafter renamed *PtRISP1*) as the most induced gene during the effective immune response to an infection by the poplar leaf rust pathogen *Melampsora larici-populina* (Rinaldi et al., 2007). *PtRISP1* is cationic, thermostable, composed of 60 amino acids in its mature form, and secreted into the apoplast in *Nicotiana benthamiana* (Petre et al., 2016). Previous circular dichroism and NMR analyses showed that *PtRISP1* is intrinsically disordered. Biochemical analyses also showed that *PtRISP1* is monomeric, probably forms two disulfide bonds, and the redox state of the cysteine residues

does not affect its properties and activities. Importantly, we previously showed that both untagged and hexahistidine-tagged *PtRISP1* purified from *Escherichia coli* directly inhibit the growth of *M. larici-populina* both *in vitro* and on poplar, and trigger poplar cell culture alkalinization in a dose-dependent manner (Petre et al., 2016). The *PtRISP1* gene resides next to an *LRR-RP* gene (hereafter named *Populus trichocarpa RISP-ASSOCIATED LRR-RP*; *PtRALR*), and both genes are co-regulated in response to biotic or abiotic stress (Petre et al., 2014). Such observations led us to hypothesize that *PtRISP1* and *PtRALR* proteins are functionally connected.

The present study aimed at evaluating the diversity and evolution of *RISP* and *RALR* gene families in *Salicaceae*, and at determining whether *RISPs* activate plant immune signaling in a *RALR*-dependent manner. To reach the first objective, we used a phylogenomic approach to make an inventory of and analyze *RISP* and *RALR* genes in *Salicaceae*. To reach the second objective, we combined protein biochemistry with *in vitro* and *in planta* assays to functionally characterize a *RISP* from willow (*Salix purpurea* *RISP1*; hereafter *SpRISP1*) and to evaluate the ability of *PtRISP1* and *SpRISP1* to trigger immune signaling in leaves expressing their clustered *RALR*. Overall, this study concludes that *RISP* and *RALR* genes belong to gene families that specifically evolved as clusters in poplar and willow, and that two divergent *RISP*–*RALR* pairs from poplar and willow cooperate to trigger immune signaling.

Materials and methods

Biological material

Nicotiana benthamiana plants were grown from seeds obtained in-house in soil at 23 °C either in a phytotron chamber for confocal microscopy assays (60% relative humidity, and a 16 h photoperiod at 400 $\mu\text{mol s}^{-1} \text{m}^{-2}$) or in a greenhouse for ROS burst and MAPK activation assays. Poplar hybrids (*Populus tremula* × *Populus alba* clone INRAE 717-1B4) were propagated *in vitro* in test tubes from internodes transplanted in sterile Murashige and Skoog (MS) medium at pH 5.9–6.0 complemented with 10 ml l^{-1} vitamin solution (100 mg l^{-1} nicotinic acid, pyridoxine HCl, thiamine, calcium pantothenate, L-cysteine hydrochloride, and 1 ml of biotin solution at 0.1 mg ml^{-1} in 95% ethanol) in a growth chamber at 23 °C and with a 16 h photoperiod at 50 $\mu\text{mol s}^{-1} \text{m}^{-2}$. The *E. coli* strain BL21 (DE3) psBET and the *Agrobacterium tumefaciens* strain GV3101 (pMP90) were used for protein production for purification and for the transient protein expression in *N. benthamiana*, respectively. Urediniospores of *M. larici-populina* (isolate 98AG31) were obtained as previously described (Rinaldi et al., 2007) and stored as aliquots at –80 °C.

In silico sequence analyses

To identify *RISP* and *RALR* genes in *Salicaceae* genomes, we searched the predicted proteomes of seven *Salicaceae* individuals available on Phytozome v13 (<https://phytozome-next.jgi.doe.gov/>), using the BlastP tool and employing the amino acid sequences of *PtRISP1* or *PtRALR* as queries (Supplementary Datasets S1, S2). We also searched the NCBI nr database as well as all available predicted proteomes on the Phytozome portal for additional sequences. The relative positions of *RISP* and *RALR* genes in the genomes were estimated with the JBrowse tool on the Phytozome portal. The sequences of RPL30, RXEG1, Cf9, RPL23, and INR were

retrieved from the UniProt and The Arabidopsis Information Resource (TAIR) databases. All the sequences used in this study are archived in Supplementary Datasets S1 and S2. *Salicaceae*-specific LRR-RP sequences were obtained from a previous study (Petre *et al.*, 2014) or identified within the predicted proteome of *S. purpurea* on the Phytozome portal.

Plasmid construction

Binary vectors were built using the Golden Gate modular cloning technology, with cloning kits and protocols described previously (Weber *et al.*, 2011; Engler *et al.*, 2014; Petre *et al.*, 2017). Briefly, coding sequences were obtained by DNA synthesis (Genecust S.A.S, BOYNES, France) or PCR cloning from poplar cDNAs and then subcloned into pAGM1287 vectors to create level 0 modules with AATG–TTCG compatible overhangs. The level 0 module was then assembled into a level 1 binary vector (pICH47742 or vector from the same series), along with a short version of the 35S promoter (pICH51277; GGAG–AATG compatible overhangs), the coding sequence of a C-terminal tag such as a mCherry (pICSL50004; AATG–GCTT compatible overhangs) or a green fluorescent protein (GFP) (pICSL50008; AATG–GCTT compatible overhangs), and a combined 3' untranslated region (UTR)/OCS terminator (pICH41432; GCTT–CGCT compatible overhangs) (Supplementary Dataset S3; Supplementary Fig. S1A). The coding sequence of the P19 suppressor of gene silencing (pICH44022, AATG–GCTT compatible overhangs) was assembled into a level 1 binary vector (pICH47761) along with a short version of the 35S promoter and a combined 3' UTR/OCS terminator (Jay *et al.*, 2023). Multigene (i.e. level 2) vectors were built by combining DNA fragments from appropriate and compatible level 1 vectors (Supplementary Fig. S2). Vectors for bacterial protein expression were built using the restriction/ligation technology and a collection of pET vectors as previously described (Petre *et al.*, 2016). Briefly, the coding sequence of the mature (without signal peptide) form of SpRISP1 was obtained by DNA synthesis directly cloned into the pET15b vector (insert between *Nde*I/*Bam*H I restriction sites), with an N-terminal hexahistidine tag encoded by the vector replacing the predicted signal peptide (Genecust S.A.S, BOYNES, France) (Supplementary Fig. S1A). All purified plasmids were stored in double distilled water at –20 °C until further use. All vectors obtained and used in this study are listed in Supplementary Dataset S3, along with the amino acid sequence of relevant proteins.

Phylogenetic analyses

To build phylogenetic trees, we used a five-step pipeline. Firstly, we performed an amino acid alignment using the muscle algorithm implemented in the Seaview software (Gouy *et al.*, 2010). Secondly, we used this alignment to identify the best substitution model with the IQTREE web server (Trifinopoulos *et al.*, 2016). Thirdly, we selected suitable positions to build a tree in the alignment of the first step with the Gblock algorithm (for RISPs) or selected the positions matching the C3-D domain (for LRR-RPs). Fourthly, we built a maximum likelihood tree (PhyML tool, with model identified in step 2, 100–1000 bootstraps, and default parameters) and archived unrooted trees as text files (Supplementary Dataset S4). Finally, we used the graphical software Figtree (<http://tree.bio.ed.ac.uk/software/figtree/>) as well as Microsoft PowerPoint to analyze and render final trees displayed in the manuscript.

Protein expression in *E. coli* and purification by affinity chromatography

PtRISP1 expression and two-step (affinity chromatography–differential precipitation to heat treatment) purification was carried out as described previously in Petre *et al.* (2016). To express proteins in the cytosol of *E. coli*, we inserted pET15b vectors into *E. coli* strain BL21 (DE3) psBET and selected transformants on solid LB broth with appropriate antibiotics

at 37 °C. Protein expression was induced during the exponential phase of growth of the bacteria by adding isopropyl-β-D-thiogalactopyranoside (IPTG) to the bacterial culture at a final concentration of 100 μM for 4 h at 37 °C. The bacterial cultures were then centrifuged for 15 min at 8000 g at 4 °C. Pellets were resuspended in 15 ml of TE-NaCl buffer (50 mM Tris–HCl pH 8.0, 1 mM EDTA, 100 mM NaCl) and stored at –20 °C. To purify the histidine-tagged proteins, the pellets were sonicated, and the soluble and insoluble fractions were separated by centrifugation for 30 min at 50 000 g at 4 °C. The soluble fractions were loaded onto an immobilized-metal affinity chromatography (IMAC) column (Ni Sepharose™ 6 Fast Flow, Cytiva, Sweden) using a peristaltic pump. Successive washing steps were performed with a washing buffer (50 mM Tris–HCl pH 8.0, 300 mM NaCl, 20 mM imidazole) to remove contaminants. Proteins were eluted using 20 ml of elution buffer (50 mM Tris–HCl pH 8.0, 300 mM NaCl, 250 mM imidazole) and concentrated to 1–2 ml by ultrafiltration using a Vivaspin® Turbo Centrifugal Concentrator (Sartorius, UK). To remove imidazole and potential contaminants (e.g. small molecules, salts, and short peptides), proteins were transferred into a dialysis membrane (Standard RC Tubing, MWCO: 6–8 kDa, diameter 6.4 mm, Spectrum Laboratories, Inc.) and incubated under agitation in imidazole-free dialysis buffer (30 mM Tris–HCl pH 8.0, 200 mM NaCl, 1 mM EDTA; 30 mM Tris–HCl pH 8.0, 1 mM EDTA; or pure water) overnight and two additional hours in a new dialysis solution. This dialysis process dilutes imidazole ~10 000 times, resulting in a final theoretical imidazole concentration of 25 μM compatible with antimicrobial assays. Finally, PtRISP1 proteins were incubated at 95 °C for 15 min in microcentrifuge tubes, and heat-aggregated proteins were removed by centrifugation at 12 000 g for 10 min (GFP did not undergo the heating step). Protein final concentration was determined by a spectrophotometric analysis of protein absorbance at 280 nm, and protein purity and integrity were estimated by 15% SDS–PAGE/CCB (Coomassie brilliant blue) staining (Supplementary Fig. S1B). Purified proteins were stored at 4 °C and used within 30 d. Before every subsequent assay, proteins were centrifuged at 12 000 g for 10 min to pellet and remove potential aggregates, and their concentration was re-assessed by spectrophotometry.

Thermostability, pull-down, and inhibition of spore germination assays

Protein thermostability, pull-down, and *in vitro* inhibition of spore germination assays were performed as described previously in Petre *et al.* (2016). Briefly, to perform the protein thermostability assay, purified proteins were incubated for 10 min at 95 °C, centrifuged to pellet aggregated proteins, and the supernatant containing the soluble proteins was collected. Proteins were then visualized by 15% acrylamide SDS–PAGE followed by CBB staining. Purified PtRISP1 and GFP were used in these bioassays as positive and negative controls, respectively. Briefly, to perform pull-down assays, 50 μg of purified proteins were incubated with *M. larici-populina* urediniospores for 15 min in 0.05% Tween-20 in water under inversion, washed twice in 0.05% Tween-20 solutions by centrifugation, and finally eluted in 100 μl of Laemmli buffer. Briefly, to perform *in vitro* inhibition of spore germination assays, purified proteins (100 μM) and *M. larici-populina* urediniospores were mixed in a microcentrifuge tube for 1 min, then 100 μl of the spore–protein mixture was plated on ~30 ml of solid water–1% agar medium in a Petri dish. After a minimum of 6 h of incubation at room temperature, the germination status of a minimum of 300 spores per condition was determined by light microscopy.

Transient protein expression in *N. benthamiana*, laser-scanning confocal microscopy assays, and image analysis

Transient protein expression and confocal microscopy were performed as previously described (Petre *et al.*, 2017). Briefly, binary vectors were

inserted into *A. tumefaciens* strain GV3101 (pMP90); the bacteria carrying the vector were then infiltrated in the leaves of 3- to 5-week-old *N. benthamiana* plants. Microscopy analyses were performed with a ZEISS LSM 780 (Zeiss International) laser-scanning confocal microscope with the $\times 40$ objective using the methods for image acquisition and interpretation described in Petre *et al.* (2021). The fluorescence of GFP, mCherry, and chlorophyll was observed using the following excitation/emission wavelengths: 488/500–525 nm, 561/580–620 nm, and 488/680–700 nm, respectively. The fluorescence intensity was measured by using the ‘Measure’ tool on Fiji software (<https://fiji.sc/>), and data were exported in a spreadsheet and analyzed with Microsoft Excel.

Mitogen-activated protein kinase activation assays

Leaf disks of *N. benthamiana* transiently expressing RALR and PtSOBIR1 were harvested 3 d post-infiltration with a biopsy punch (8 mm diameter). Eight leaf disks were infiltrated with 1 μM flg22 or 100 μM of purified PtRISP1/SpRISP1 and incubated for 0, 15, or 30 min prior to flash-freezing and grinding in liquid nitrogen. Proteins were extracted by incubation of the leaf powder in Laemmli buffer (62.5 mM Tris–HCl pH 6.8, 8.3% glycerol, 2% SDS, 0.017% bromophenol blue) with 100 mM DTT for 10 min at 95 °C. The samples were centrifuged at 12 000 g and the proteins were separated by SDS-PAGE. Proteins were then transferred onto a polyvinylidene fluoride (PVDF) membrane, which was subsequently incubated with the primary antibody α -pMAPK for at least 1 h [Phospho-p44/42 MAPK (erk1/2) 1:5000; Cell Signaling Technology] and then with the secondary antibody (Sigma anti-rabbit 1:10 000) until observation of a detectable signal with a ChemiDoc Imaging System (Bio-Rad). CBB staining of the proteins on the membranes was used as a loading control.

Reactive oxygen species burst assay

Leaf disks of *N. benthamiana* transiently expressing RALR and PtSOBIR1 were harvested 3 d post-infiltration with a biopsy punch (4 mm diameter). Disks were placed in a 96-well plate, incubated in 100 μl of distilled water, and kept at room temperature overnight. Prior to the ROS quantification, water was replaced with 100 μl of assay solution [0.5 μM L-012, 10 $\mu\text{g ml}^{-1}$ horseradish peroxidase (HRP), 100 nM flg22 in water or 100 μM of purified RISP, or TE buffer pH 8] and light emission was measured immediately with a Spark microplate reader (Tecan, Switzerland). Relative light units (RLUs) were collected in 60 s intervals for 60 min or 90 min. Data were exported in a spreadsheet and analyzed with Microsoft Excel.

Stomatal closure assay

Stomatal closure assay was performed with leaves of 3- to 5-month-old plants of *P. tremula* \times *P. alba* clone INRAE 717-1B4 grown *in vitro*. Full leaves were harvested and incubated in a stomata opening buffer (10 mM MES, 50 mM KCl, pH 6.15) (Liu *et al.*, 2021) for 2 h under light (50 $\mu\text{mol m}^{-2} \text{s}^{-1}$). Leaves were then incubated for 2 h in purified PtRISP1 or GFP to a final concentration of 100 μM , in water under light conditions (open stomata control), or in water under dark conditions (closed stomata control). Leaves were then mounted in water between a glass slide and a cover slip, and images of randomly selected positions of the abaxial side of the leaves were recorded with a light microscope with a $\times 40$ water immersion objective and a camera (Lordil). The stomatal opening widths and lengths were measured on images using Fiji, and the width/length ratio was calculated to evaluate the stomatal aperture (raw data are available in Supplementary Dataset S5). Statistical analyses were performed on RStudio using Wilcoxon rank sum test with continuity correction.

Results

Clusters of *RISP* and *RALR* genes evolved specifically in *Salicaceae*

To determine if PtRISP1 belongs to a gene family, we comprehensively searched for PtRISP1 homologs in publicly available predicted proteomes. In total, the search identified 24 such homologs (hereafter RISPs) in eight different genomes of seven *Salicaceae* species (Supplementary Dataset S1). Those 24 *RISP* genes group among eight clusters of 2–4 genes harbored by chromosome 9 (one cluster per genome), except for *P. trichocarpa* which presents two clusters (a second cluster being present on the small scaffold 502). The 24 RISP family members vary in size from 76 to 83 amino acids (50–58 amino acids in their mature form) and exhibit an average percentage identity of 68% (Fig. 1A). We found no RISP outside poplar or willow, suggesting that the RISP family evolved specifically in *Salicaceae* species. The phylogenetic analysis shows that poplar and willow RISPs group into two well-supported phylogenetic clades, suggesting that the family evolved from a single ancestral gene that emerged in the ancestor species of poplars and willows ~60 million years ago (Fig. 1A) (Liu *et al.*, 2022). RISP predicted signal peptides are highly conserved (mean p-distance of 0.158 ± 0.11), whereas RISP mature forms differ more (mean p-distance of 0.458 ± 0.18). Despite this sequence variability, RISP mature forms present four regions with noticeable and conserved properties: (i) an N-terminal region with a predicted α -helical structure; (ii) a hydrophilic region; (iii) a positively charged region (average net positive charge of 6 ± 1.6); and (iv) a C-terminal negatively charged region (average net negative charge of 2.7 ± 0.8) (Fig. 1A; Supplementary Dataset S1). Also, RISPs have four fully conserved cysteines in their mature form and present high predicted isoelectric points (average of 9.5 ± 0.3) (Fig. 1A). Altogether, these results suggest that RISP evolved as clusters, specifically and recently in *Salicaceae* species to form a diverse family of cationic secreted peptides.

To evaluate how *PtRALR* evolved within the *LRR-RP* gene family, we comprehensively searched for *PtRALR* homologs in publicly available predicted proteomes as well as in the NCBI protein database. In total, this search identified only 25 such homologs (hereafter RALRs) belonging to 10 different *Salicaceae* species (Supplementary Dataset S2). The 25 RALRs display an average amino acid similarity of 88.5% (ranging from 70% to 99.5%) and an average length of 1060 amino acids (ranging from 1045 to 1075; *PtRALR* comprising 1046 amino acids). All RALRs gather into a well-separated clade (hereafter the RALR clade) within a phylogenetic tree of LRR-RPs; the RALR clade itself resides within a large clade of *Salicaceae* LRR-RPs. Within the RALR clade, the willow sequences gather into a separate subclade (Fig. 1B). Interestingly, among the 25 RALRs, eight originate from the eight *Salicaceae* genomes present on the Phytozome portal; those eight *RALR* genes all reside within the *RISP* clusters, immediately downstream of

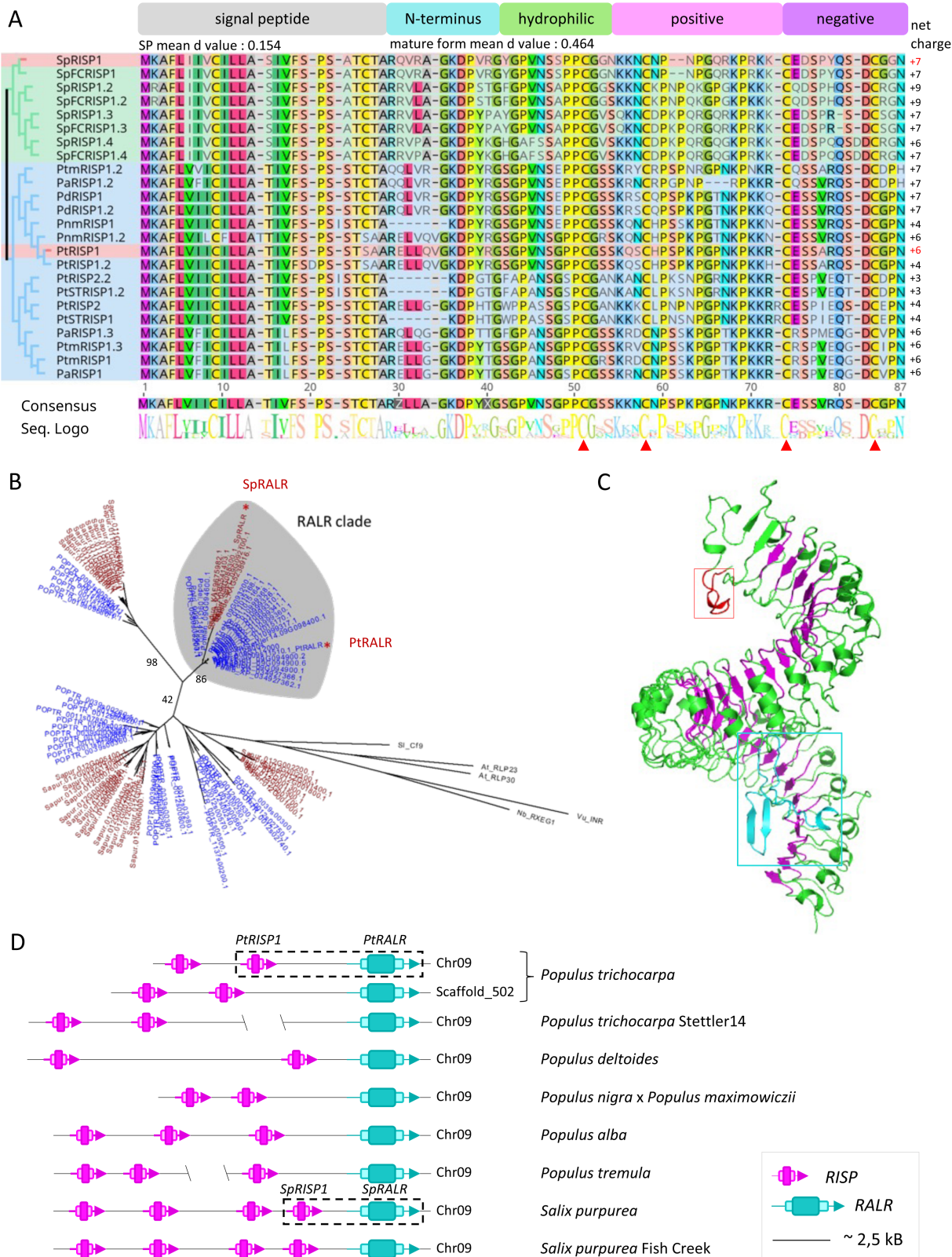


Fig. 1. Clusters comprising RISP and RALR genes evolved specifically in Salicaceae. (A) Alignment of 24 RISP amino acid sequences identified in the Salicaceae genomes. The alignment matches the phylogenetic tree represented on the left side: *Populus* and *Salix* sequences are highlighted in blue and green, respectively (Supplementary Datasets S1, S4). The two RISPs investigated in this study are highlighted in red. At the top of the alignment,

five regions with various properties were identified: a predicted signal peptide (gray box), an N-terminal region (blue box), a hydrophilic region (green box), a positively charged region (pink box), and a negatively charged region (purple box). At the bottom of the alignment, the consensus sequence and the web logo are represented; the red arrowheads point to the four highly conserved cysteines. The net charge for each peptide is indicated (column on the right). (B) Phylogenetic tree generated from *Populus* (blue) and *Salix* (red) LRR-RPs as well as selected LRR-RPs from model plants (*Arabidopsis thaliana*, *Nicotiana benthamiana*, *Solanum lycopersicum*, and *Vigna unguiculata*) (black; outgroup). All RALRs gather into a well-separated clade (RALR clade highlighted in gray). Within the RALR clade, the willow sequences gather into a separate subclade. Red dots point to SpRALR and PtRALR. (C) AlphaFold2-predicted tridimensional model of PtRALR, with the leucine-rich repeat region in green and the LRR motifs in pink (pLDDT=83.1). The red and blue squares indicate the N-loopout (red) and the island domain (cyan), respectively. A movie and additional 3D models are available in [Supplementary Fig. S4](#). (D) Schematic representation of the clusters of *RISP* (magenta) and *RALR* (cyan) genes on the chromosomes or scaffolds in the genomes of *P. trichocarpa*, *P. trichocarpa* Stettler14, *P. deltoides*, *P. nigra* × *P. maximowiczii*, *P. tremula* × *P. alba* (tremula or alba haplotypes), *S. purpurea*, and *S. purpurea* Fish Creek. Raw data are available in [Supplementary Datasets S1, S2](#), and [S4](#).

the *RISP* genes ([Fig. 1D](#); [Supplementary Dataset S6](#)). Thus, all *RISP* and *RALR* genes identified in the available *Salicaceae* genomes so far cluster together, in such a way that the clusters comprise one *RALR* gene and 2–4 *RISP* genes. Overall, these findings suggest that clusters comprising *RISP* and *RALR* genes evolved and diversified from a common ancestor cluster in *Salicaceae* species.

We hypothesized that the products of *RISP* and *RALR* genes present in the same cluster function together to trigger immune signaling. To test this hypothesis, we selected two pairs of clustered *RISP* and *RALR* genes: *PtRISP1*–*PtRALR* in poplar and *SpRISP1*–*SpRALR* in willow ([Fig. 1D](#); [Supplementary Fig. S3](#)). Both pairs encode divergent proteins, as the mature forms of *PtRISP1* and *SpRISP1* as well as *PtRALR* and *SpRALR* exhibit only 59% and 85% amino acid identity, respectively ([Supplementary Fig. S3](#)). *PtRALR* and *SpRALR* present all the canonical domains of LRR-RPs: a predicted N-terminal signal peptide, a cysteine-rich domain, a leucine-rich repeat region with 33 LRRs, an acid-rich domain, a transmembrane helix, and a cytosolic tail ([Fig. 1C](#); [Supplementary Figs S4, S5](#)). The AlphaFold2-generated tridimensional models of both *PtRALR* and *SpRALR* predict the canonical superhelix fold of the LRR domain, that comprises the N-terminal loop (N-loopout) and C-terminal island domain (ID) involved in ligand recognition in other LRR-RPs ([Fig. 1C](#); [Supplementary Figs S4, S5](#)) ([Matsushima and Miyashita, 2012](#); [Sun et al., 2022](#); [Snoeck et al., 2023](#)).

SpRISP1 exhibits biophysical properties and antimicrobial activities similar to PtRISP1

A previous study showed that *PtRISP1* accumulates in the apoplast in *N. benthamiana*, is thermostable, and binds and inhibits the germination of urediniospores of *M. larici-populina* ([Petre et al., 2016](#)). We aimed at determining whether SpRISP1 presents similar biophysical properties and antimicrobial activities. To this end, we first transiently expressed an SpRISP1–mCherry fusion in *N. benthamiana* leaves and determined its accumulation pattern by laser scanning confocal microscopy. This analysis showed that SpRISP1 and PtRISP1 (used as a positive control) exclusively accumulate in the apoplast without overlapping with the signal of a free GFP (used

as a nucleo-cytoplasmic marker) ([Fig. 2A](#)). In addition, western blot analyses revealed the presence of RISP–mCherry fusions and SP-Ramya3A–mCherry (apoplastic control) in apoplastic fluids from *N. benthamiana* leaves, whereas intracellular GFP was only detected in total leaf protein extracts ([Supplementary Fig. S6](#)). Then, we obtained the mature form of SpRISP1 as a purified protein produced in *E. coli* and observed that the protein remains soluble after heat treatment for 10 min at 95 °C, similar to PtRISP1 ([Fig. 2B](#)). Pull-down assays showed that SpRISP1 attaches to urediniospores, similar to PtRISP1 (positive control), whereas a GFP negative control did not ([Fig. 2C](#)). Finally, inhibition of germination assays revealed that a solution of 100 μM SpRISP1 inhibited the germination of *M. larici-populina* urediniospores, similar to a PtRISP1 positive control (germination rates of 22 ± 7% and 8.5 ± 6%, respectively), as opposed to the mock treatment which had a high germination rate of >85 ± 8% ([Fig. 2D](#)). Altogether, these results indicate that SpRISP1 accumulates in the apoplast, is thermostable, and interacts with *M. larici-populina* urediniospores and inhibits their germination. As PtRISP1 and SpRISP1 belong to the two major and divergent subclades of their family, these findings suggest that RISP family members evolved similar biophysical properties and activities.

PtRALR and SpRALR accumulate at the plasma membrane in *N. benthamiana*

To functionally investigate the ability of RALRs to recognize RISPs, we used transient expression assays in *N. benthamiana* (as *Salicaceae* species are limitedly amenable to reverse genetics). Firstly, we aimed at accumulating RALR–GFP fusions in leaf cells to characterize their subcellular localization, by co-expressing PtRALR–GFP or SpRALR–GFP fusions with PtRISP1–mCherry (used as an apoplastic marker) and the P19 protein (a silencing suppressor) in leaves by agroinfiltration. This assay revealed a weak GFP signal at the cell periphery, which did not overlap with the mCherry signal ([Fig. 3](#)). Of note, the accumulation of RALR–GFP fusions required the presence of the P19 protein, as we observed no fluorescent signal in assays without P19. These first results indicate that RALR–GFP fusions can accumulate in *N. benthamiana*, but at low levels, which precludes further functional analyses.

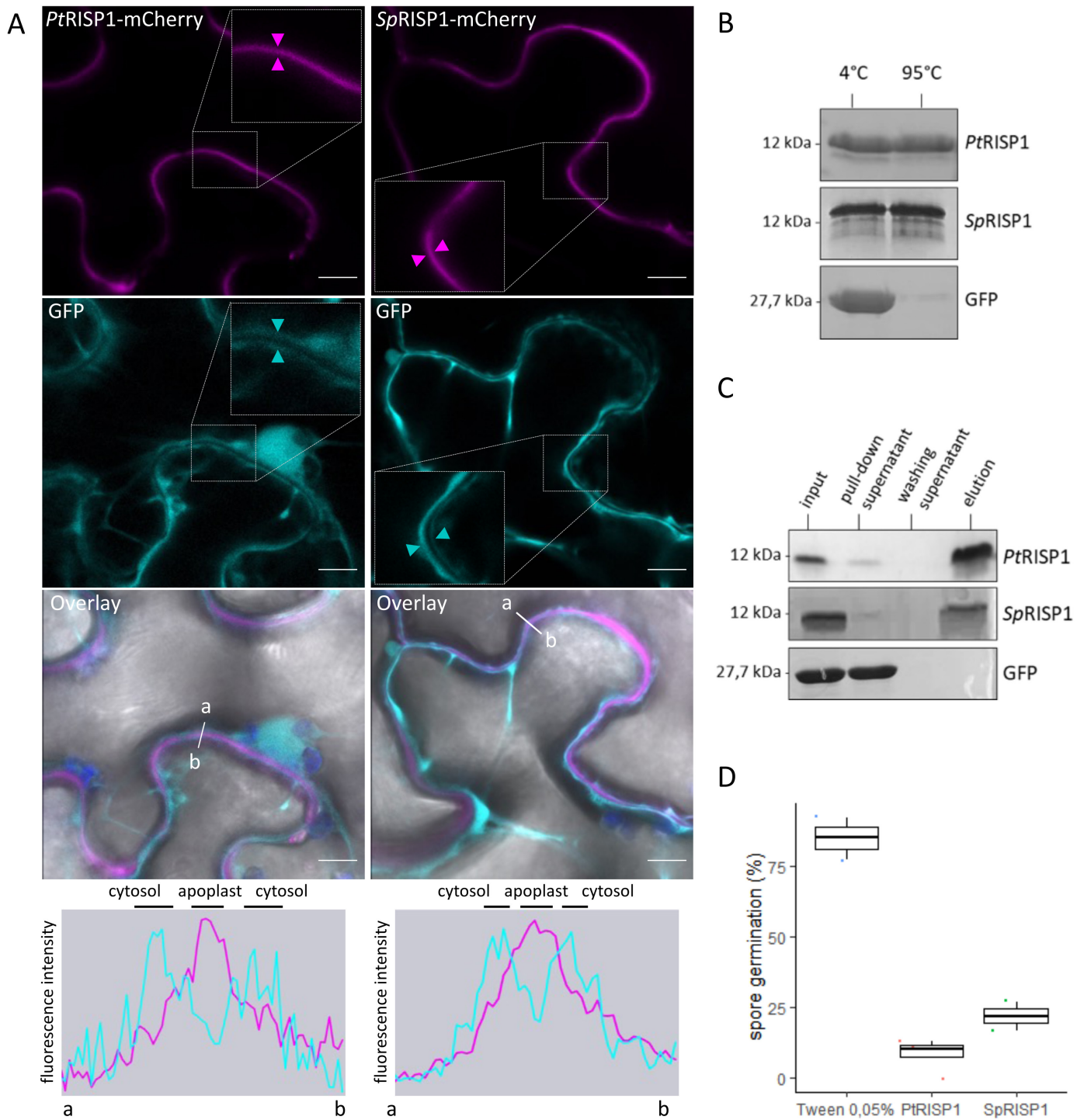


Fig. 2. SpRISP1 shows biophysical properties and antimicrobial activities that are similar to PtRISP1. (A) SpRISP1 accumulates in the apoplast. Confocal microscopy images of *N. benthamiana* leaf epidermal cells transiently co-accumulating SpRISP1-mCherry or PtRISP1-mCherry (in cyan) with a free GFP (in magenta) used as a nucleo-cytoplasmic marker, acquired through three independent agroinfiltration assays. Scale bars=10 μ m. Image inserts show $\times 2$ zoomed areas, the magenta arrowhead indicates the apoplast; the cyan arrowheads indicate cytosols. Fluorescence intensity graphs show mCherry (magenta) and GFP (cyan) signals measured along the white line from a to b. Detection of both RISP-mCherry fusions in the apoplastic fluid from *N. benthamiana* leaves is shown in [Supplementary Fig. S6](#). (B) SpRISP1 is thermostable. Purified proteins were incubated at 95 °C for 10 min; soluble proteins before (4 °C) or after heating (95 °C) were visualized by SDS-PAGE/CBB staining. (C) SpRISP1 interacts with *Melampsora larici-populina* urediniospores *in vitro*. Purified proteins of the different fractions collected were visualized by SDS-PAGE/CBB staining. Input: protein solution before centrifugation. Pull-down supernatant: supernatant after the first centrifugation. Washing supernatant: supernatant after the second centrifugation for washing. Elution: supernatant after incubation at 95 °C in Laemmli buffer. (D) SpRISP1 inhibits *M.*

larici-populina urediniospore germination. *In vitro* inhibition of germination assays was performed on water–agar medium with 100 μ M purified PtRISP1 or SpRISP1 boiled for 10 min at 95 °C, or with 0.05% Tween-20 (mock treatment). The percentage germination was determined after a minimum of 6 h of incubation. For further details regarding the inhibition of spore germination by PtRISP1, control conditions, and related assays, we refer readers to our previous study (Petre et al., 2016).

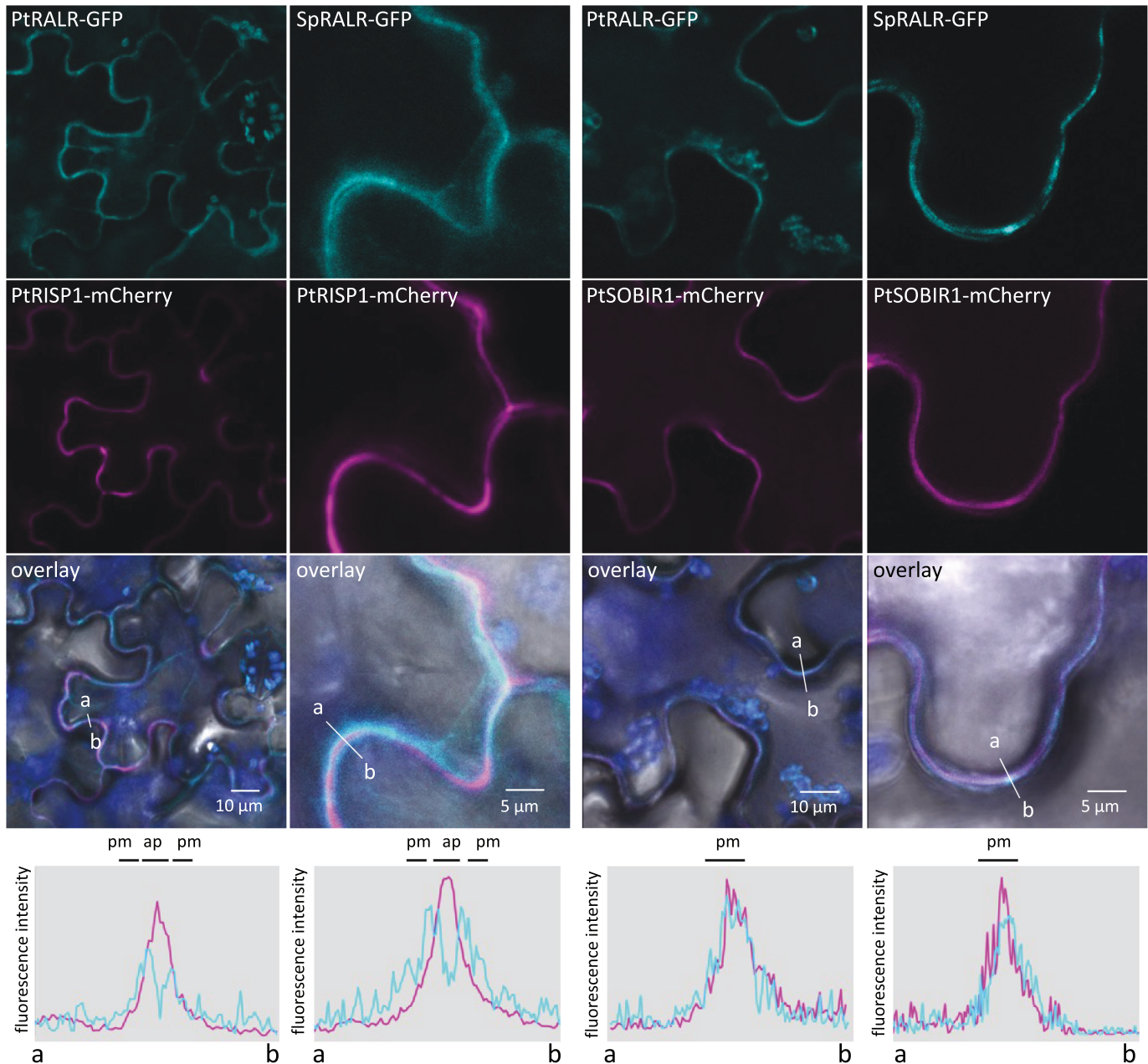


Fig. 3. PtRALR and SpRALR accumulate at the plasma membrane in *N. benthamiana*. Confocal microscopy images of *N. benthamiana* leaf epidermal cells transiently co-accumulating PtRALR-GFP and SpRALR-GFP (cyan images on top), PtRISP1-mCherry as apoplastic marker or PtSOBIR1-mCherry as plasma membrane marker (magenta images in the middle), and P19 (suppressor of gene silencing) protein. Live cell imaging was performed with a confocal microscope 3 d after infiltration. The overlay images combine the GFP, mCherry, chlorophyll (blue), and bright field. Scale bars=5 μ m or 10 μ m. Fluorescence intensity graphs show mCherry (magenta) and GFP (cyan) signals measured along the white line from a to b.

The presence of the adaptor kinase SOBIR1 was shown to assist the accumulation of LRR-RPs in plant cells (Liebrand *et al.*, 2013, 2014; Böhm *et al.*, 2014). To improve our ability to express RALR–GFP fusions in *N. benthamiana*, we aimed at co-expressing them with a homolog of SOBIR1 from a *Salicaceae* species. To this end, we cloned the coding sequence of one of the two SOBIR1 homologs in *P. trichocarpa* (PtSOBIR1). PtSOBIR1 shares 64% and 66% amino acid identity with SOBIR1 sequences from *Arabidopsis thaliana* and *N. benthamiana*, respectively, and comprises both a conserved C-terminus and a GXXXG dimerization motif in the transmembrane domain (Bi *et al.*, 2016) (Supplementary Fig. S7). As PtSOBIR1 shares high amino acid identity (88%) with its closest homolog in *Salix*, we used PtSOBIR1 for the assays with SpRALR. As anticipated, PtSOBIR1–mCherry fusions clearly and specifically accumulated at the plasma membrane in *N. benthamiana* (Supplementary Fig. S8A). Co-expression of RALR–GFP, P19, and PtSOBIR1–mCherry fusions revealed a well-detectable co-accumulation of fluorescent signals at the plasma membrane (Fig. 3). Western blot analyses

revealed the presence of intact PtRALR–GFP, SpRALR–GFP, and PtSOBIR1–mCherry in leaf protein extracts (Supplementary Fig. S8B). In conclusion, these results indicate that PtRALR and SpRALR can accumulate at the plasma membrane in *N. benthamiana*. As no cell death or leaf stress symptoms were detectable, we surmised that transient assays would be suitable to study RALR-mediated immune signaling activation.

Purified RISPs trigger immune signaling in a RALR-dependent manner in *N. benthamiana*

To test whether RALRs are sufficient to confer RISP responsiveness to *N. benthamiana*, we combined transient assays with purified peptide treatments followed by the dynamic quantification of ROS and phosphorylated MAPKs. On the one hand, an exogenous treatment with purified PtRISP1 of leaf disks expressing PtRALR and PtSOBIR1 triggered a ROS burst that peaked at 30 min, as well as a strong accumulation of phosphorylated MAPKs 15 min and 30 min post-treatment,

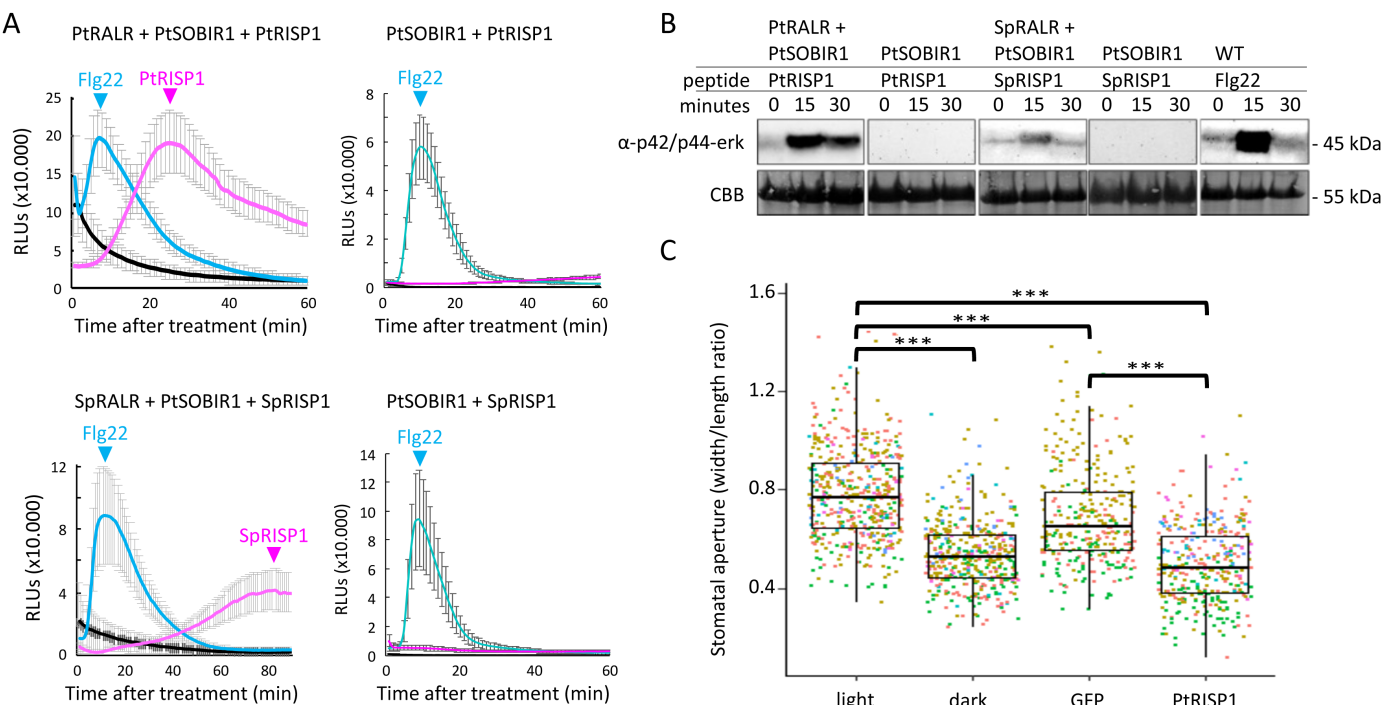


Fig. 4. RISPs induce immune signaling in RALR-expressing *N. benthamiana* and in poplar. (A) ROS accumulation was measured in *N. benthamiana* leaf disks expressing PtSOBIR1 and P19 protein alone (right-hand panel) or PtSOBIR1, P19 protein, and either PtRALR (upper left panel) or SpRALR (lower left panel). Leaf disks were treated with 100 μ M PtRISP or 100 μ M SpRISP1 (upper and lower panel, respectively; magenta), 100 nM flg22 (cyan; positive control treatment), or TE buffer (black; mock treatment). Error bars represent SEs from technical replicates ($n \geq 1$). (B) Western blot using α -p42/p44-ERK recognizing phosphorylated MAPKs isolated from *N. benthamiana* leaf disks expressing PtSOBIR1 and P19 protein alone or PtSOBIR1, P19 protein, and either PtRALR or SpRALR; WT indicates untransformed wild-type leaves. Leaf disks were treated with 100 μ M PtRISP1, 100 μ M SpRISP1, or 1 μ M flg22, respectively, for 0, 15, and 30 min. Membranes were stained with CBB as loading control. (C) PtRISP1 induces stomatal closure in *P. tremulae* and *P. alba* leaves (cultivar 717-1B4). Leaves were incubated for 2 h in water (light), in water without light (dark), or in water containing 100 μ M GFP (GFP) or PtRISP1 (PtRISP1). Images of the abaxial side of leaves were taken with a light microscope and the width/length ratio of stomata was measured using ImageJ. The different colors of the dots correspond to the six independent replicates. Asterisks stand for P -value < 0.05 from pairwise comparisons using Wilcoxon rank sum test with continuity correction ($n = 6$; 1574 stomata analyzed; raw data are available in Supplementary Dataset S5).

with intensities comparable with those triggered by the flg22 positive control (Fig. 4A, B). On the other hand, the same experiment performed with the SpRISP1–SpRALR pair revealed weaker ROS and phosphorylated MAPK accumulation, although both showed transient accumulation patterns. Neither ROS nor phosphorylated MAPKs significantly accumulated in *N. benthamiana* leaves expressing only PtSOBIR1 (Fig. 4A, B). Altogether, we conclude that the co-expression of RALRs and PtSOBIR1 in *N. benthamiana* leaves confers RISP responsiveness, suggesting that PtRALR and SpRALR recognize PtRISP1 and SpRISP1, respectively, and that this recognition rapidly initiates immune signaling events.

Purified PtRISP1 triggers stomatal closure in poplar

To determine if PtRISP1 can activate immune responses in its organism of origin, we established a stomatal closure assay in poplar. Briefly, we treated detached leaves of *in vitro* grown hybrid poplars with purified proteins for 2 h, then estimated the stomatal aperture by using the width/length ratio method (Thor et al., 2020). This assay showed that PtRISP1 treatment reduces stomatal aperture (ratio of 0.50 ± 0.16) similarly to the dark positive control (ratio of 0.54 ± 0.13), whereas leaves incubated with a GFP purified in parallel to PtRISP1 (used as a proteinaceous negative control) or with a mock treatment showed a higher stomatal aperture (ratio of 0.69 ± 0.2 and 0.78 ± 0.19 , respectively) (Fig. 4C). Statistical analyses indicated that stomatal aperture was significantly different between PtRISP1, light condition, and GFP, whereas no significant difference was observed between PtRISP1 and the dark condition used as a positive control. Thus, exogenous treatment of PtRISP1 triggers a rapid and strong stomatal closure, suggesting that PtRISP1 is sufficient to elicit an immune-related response in poplar leaves.

Discussion

This study reports that clusters of *RISP* and *RALR* genes evolved recently and specifically in *Salicaceae* species, and that RISP family members function as defense peptides with both antifungal and elicitor activities, with the elicitor activity being dependent on their clustered RALR. This section discusses the multifunctionality of plant defense peptides, the surprising clustering of genes encoding cooperating peptides and cell surface proteins in plants, the efforts required for the characterization of LRR-RPs in non-model species, and the original position of RALRs as LRR-RPs required for a phytocytokine activity.

The characterization of plant functional analogs of metazoan host defense peptides emerges as a research front

We showed that RISP family members simultaneously exhibit antimicrobial and immunomodulatory activities,

making RISPs functional analogs of metazoan HDPs. The characterization of HDP analogs in plants is emerging as a research front (Petre, 2020; Han et al., 2023). Notably, recent studies have reported two superfamilies of plant defense peptides, namely PATHOGENESIS-RELATED PROTEIN 1 (PR1) and SERINE RICH ENDOGENOUS PEPTIDES (SCOOPs), with members having antimicrobial and immunomodulatory activities (Neukermans et al., 2015; Yu et al., 2020; Guillou et al., 2022; Han et al., 2023). PR1 superfamily members are well-characterized inhibitors of microbial growth (Niderman et al., 1995), and PR1 is cleaved to release the C-terminal CAP-derived peptides (CAPEs) that activates plant immune responses (Chen et al., 2014, 2023; Sung et al., 2021). PR1 superfamily members are also targeted by pathogen effectors that prevent CAPE1 cleavage, demonstrating the importance of this process in plant immunity (Lu et al., 2014; Sung et al., 2021). Furthermore, the divergent superfamily of SCOOPs comprises members exhibiting antifungal activities (Neukermans et al., 2015; Yu et al., 2020). SCOOP peptides are recognized by the *A. thaliana* LRR-RK MALE DISCOVERER 1-INTERACTING RECEPTOR LIKE KINASE 2 (MIK2) to induce immunity (Hou et al., 2021; Rhodes et al., 2021; Zhang et al., 2022). In addition to these two well-studied families, defensin and thaumatin-like protein families may also harbor functional analogs of HDPs (Petre, 2020). Future studies on plant multifunctional immune peptides may help reveal their valorization potential in agriculture as versatile ‘Swiss-army knife’ molecules (Hilchie et al., 2013; Sun et al., 2023). Such studies could also improve our understanding of the eukaryotic immune systems, for instance by highlighting how metazoans and plants evolved functionally analogous defense peptides.

Can gene clustering analyses help to identify cooperating phytocytokines and cell surface proteins?

A pilot study screened the poplar genome to reveal that *PtRISP1* and *PtRALR* genes cluster together, and speculated on a functional link between the two (Petre et al., 2014). In this follow-up study, we showed that *RISP* and *RALR* gene family members systematically cluster, and that at least two RISP–RALR pairs function together to trigger immune signaling. The direct clustering of genes encoding phytocytokines and RRs or RPs is not common. For instance, in *A. thaliana*, the genes encoding well-characterized phytocytokine–RK pairs, such as PEP1–PEPR1, PIP1–RLK7, or SCOOP12–MIK2, reside on different chromosomes. Indeed, *PEP1*, *PIP1*, and *SCOOP12* genes are located on chromosomes 2, 3, and 5, respectively, whereas the genes encoding the matching RRs are all located on chromosome 1 in the *A. thaliana* genome (Supplementary Dataset S6) (Rzemieniewski and Stegmann, 2022). Identifying cooperating pairs of regulatory peptides and cell surface proteins

is a central goal in both plant and animal biology, though such an endeavor requires experimentally demanding and time-consuming screening approaches (Ramilowski *et al.*, 2015; Boutrrot and Zipfel, 2017; Siepe *et al.*, 2022). Screening genomes for physically associated and co-regulated genes encoding cell surface proteins and small secreted proteins may help accelerate the identification of ligand–receptor pair candidates.

Characterizing LRR-RPs from non-model species requires significant efforts to gain genome-wide family knowledge, produce molecular material, and implement methodologies

Our study initiated the characterization of LRR-RPs in two species of the *Salicaceae* family. The 19 immunity-related LRR-RPs characterized so far belong to only three plant families: *Solanaceae* (12), *Brassicaceae* (6), and *Fabaceae* (1) (Snoeck *et al.*, 2023). Though poplar and willow are considered as model trees, they lack strong reverse genetic tools and remain underinvestigated compared with annual models (Marks *et al.*, 2023). For instance, rapid transient expression assays are still lacking and cannot be systematically applied. Characterizing LRR-RPs from non-model botanical families faces the double challenge of building family-specific background knowledge and acquiring material and methodologies. We tackled the first challenge by performing a comprehensive phylogenomic analysis of LRR-RPs and structural predictions; some of this effort was included in a pilot study that was instrumental to generate hypotheses and select protein candidates (Petre *et al.*, 2014). We tackled the second challenge both by using heterologous systems (notably *N. benthamiana* to express RALRs *in planta* and *E. coli* to produce RISPs) and by implementing novel methodologies and protocols (notably the stomatal closure assay in poplar), such efforts and approaches being commonly required in non-models (Petre *et al.*, 2016; Lorrain *et al.*, 2018). The implementation of methodologies and protocols is time-consuming and often ineffective. For instance, in this study, attempts to implement bioassays were unsuccessful while consuming significant human and financial resources (i.e. gene expression induction, cell culture-based assays, and seedling growth inhibition assays). We also invested significant efforts to set up functional protein–protein interaction assays in heterologous systems to test the physical association between RALRs, RISPs, SOBIR1, and SERK3, without success so far. This experimental issue maybe be explained by the low accumulation level of RALRs in leaf cells; accumulation that, though adequate for functional assays, might not be sufficient for protein biochemistry analyses. The molecular resources and methodologies we built here will hopefully facilitate future studies addressing LRR-RPs and/or the molecular physiology of *Salicaceae*.

The LRR-RP RALR is involved in phytocytokine signaling

We showed that RISPs require RALRs to initiate immune signaling in *N. benthamiana*. To our knowledge, RALR is the first LRR-RP reported to be required for a phytocytokine activity. Indeed, known receptors of phytocytokines all belong to the superfamily of RKs (Ngou *et al.*, 2022; Rzemieniewski and Stegmann, 2022). Among the 19 immunity-related LRR-RPs, all but one are activated by pathogen-derived peptides (Snoeck *et al.*, 2023). Indeed, only INR recognizes a self-molecule—a plant-derived peptide proteolytically generated from a chloroplastic ATP synthase upon caterpillar chewing, which does not qualify as a phytocytokine *per se* (Steinbrenner *et al.*, 2020; Rzemieniewski and Stegmann, 2022). Thus, RISP–RALR pairs may serve as models to dissect the LRR-RP-mediated initiation of immune signaling by phytocytokines. To this end, the functionality of RALR in *N. benthamiana* will be instrumental, along with (i) the ability to easily biosynthesize and purify RISPs, (ii) the diversity of RISP and RALR sequences we identified to assist structure/function approaches, and (iii) the ability to predict *in silico* the structure of superhelical LRR domain of RALRs (Fig. 1; Supplementary Fig. S4). PtRISP1 was previously shown to undergo processing at its C-terminus by plant proteins (Petre *et al.*, 2016); one challenge to further dissect RISP/RALR functioning will also be to identify the exact sequence of that C-terminal peptide.

Supplementary data

The following supplementary data are available at [JXB online](#).

Fig. S1. Overview of the cloning pipeline and purification of RISPs.

Fig. S2. Schematic representation of a level 2 plasmid.

Fig. S3. Comparative analysis of PtRISP1 and SpRISP1.

Fig. S4. 3D model of PtRALR predicted using AlphaFold2.

Fig. S5. Alignment of PtRALR and SpRALR with characterized LRR-RPs

Fig. S6. Detection of RISP–mCherry fusions in the *N. benthamiana* apoplastic fluid.

Fig. S7. Sequence alignments of the SOBIR1 homologs identified in *Populus trichocarpa* and *Salix purpurea* genomes with AtSOBIR1.

Fig. S8. PtSOBIR1–mCherry fusion accumulate at the plasma membrane in *N. benthamiana*.

Dataset S1. RISP family, sequences and parameters.

Dataset S2. Amino acid sequences of the RPs used in this study.

Dataset S3. RISPs, RALRs, and PtSOBIR1 amino acid sequences, parameters, and cloning details.

Dataset S4. Archive unrooted trees of RALR and RISP sequences.

Dataset S5. Raw data of the stomatal closure assay.

Dataset S6. RISP/RALR gene clusters identified in *Salicaceae* genomes.

Acknowledgements

The authors acknowledge members of the UMR IAM, and notably N. Rouhier, M. Morel-Rouhier, C. Veneault-Fourrey, F. Lauve-Zannini, and C.P.D. Louet for fruitful discussions, C. Teissier for administrative support, M.-L. Ancel, A. Temporelli, A. Deveau, T. Dhalleine, and D. Culot-Caubriere for technical help, and P. Frey for providing material.

Author contributions

JL, CZ, SD, and BP: conceptualization, funding acquisition, and project administration; JL, YG, KWB, RB, GD, EC, and BP: data curation and formal analysis; JL, YG, KWB, RB, GD, and EC: methodology; CZ, SD, BP: supervision; JL and BP: visualization and writing—original draft; JL, YG, KWB, GD, EC, SD, CZ, and BP: writing—review and editing.

Conflict of interest

No conflict of interest declared.

Funding

This work was supported by grants overseen by the French Plan Investissement d’Avenir (PIA) Lab of Excellence ARBRE [ANR-11-LABX-0002-01], by the Pôle Scientifique A2F of the Université de Lorraine, by the Région Grand Est (France), by Lorraine Université d’Excellence (LUE) mobility programme DrEAM, by the General Programme of the European Molecular Biology Organization [EMBO Scientific Exchange Grant 9451], and by the INRAE Direction de l’Enseignement Supérieur, des Sites et de l’Europe (DESSE). Research in the Zipfel lab on phytocytokines is supported by funding from the European Research Council [grant agreement no. 773153] and by the University of Zurich. YG was supported by an EMBO Post-Doctoral Fellowship [ALTF 386-2021].

Data availability

All the material used in this study is available upon request to the corresponding author. Sequences and key information are presented in the Supplementary data.

References

- Bakare OO, Gokul A, Fadaka AO, Wu R, Niekerk LA, Barker AM, Keyster M, Klein A. 2022. Plant antimicrobial peptides (PAMPs): features, applications, production, expression and challenges. *Molecules* **27**, 3703.
- Bi G, Liebrand TWH, Bye RR, Postma J, van der Burgh AM, Robatzek S, Xu X, Joosten MH AJ. 2016. SOBIR1 requires the GxxxG dimerization motif in its transmembrane domain to form constitutive complexes with receptor-like proteins. *Molecular Plant Pathology* **17**, 96–107.
- Böhm H, Albert I, Fan L, Reinhard A, Nürnberg T. 2014. Immune receptor complexes at the plant cell surface. *Current Opinion in Plant Biology* **20**, 47–54.
- Boutrot F, Zipfel C. 2017. Function, discovery, and exploitation of plant pattern recognition receptors for broad-spectrum disease resistance. *Annual Review of Phytopathology* **55**, 257–286.
- Bradshaw HD, Ceulemans R, Davis J, Stettler R. 2000. Emerging model systems in plant biology: poplar (*Populus*) as a model forest tree. *Journal of Plant Growth Regulation* **19**, 306–313.
- Chen YL, Lee CY, Cheng KT, Chang WH, Huang RN, Nam HG, Chen YR. 2014. Quantitative peptidomics study reveals that a wound-induced peptide from PR-1 regulates immune signaling in tomato. *The Plant Cell* **26**, 4135–4148.
- Chen YL, Lin FW, Cheng KT, Chang CH, Hung SC, Efferth T, Chen YR. 2023. XCP1 cleaves pathogenesis-related protein 1 into CAPE9 for systemic immunity in *Arabidopsis*. *Nature Communications* **14**, 4697.
- DeFalco TA, Zipfel C. 2021. Molecular mechanisms of early plant pattern-triggered immune signaling. *Molecular Cell* **81**, 3449–3467.
- Duplessis S, Major I, Martin F, Séguin A. 2009. Poplar and pathogen interactions: insights from *Populus* genome-wide analyses of resistance and defense gene families and gene expression profiling. *Critical Reviews in Plant Science* **28**, 309–334.
- Engler C, Youles M, Gruetzner R, Ehnert TM, Werner S, Jones JDG, Patron NJ, Marillonnet S. 2014. A golden gate modular cloning toolbox for plants. *ACS Synthetic Biology* **3**, 839–843.
- Gouy M, Guindon S, Gascuel O. 2010. Sea view version 4: a multiplatform graphical user interface for sequence alignment and phylogenetic tree building. *Molecular Biology and Evolution* **27**, 221–224.
- Guillou MC, Balliau T, Vergne E, et al. 2022. The PROSCOOP10 gene encodes two extracellular hydroxylated peptides and impacts flowering time in *Arabidopsis*. *Plants* **11**, 3554.
- Gust AA, Felix G. 2014. Receptor like proteins associate with SOBIR1-type of adaptors to form bimolecular receptor kinases. *Current Opinion in Plant Biology* **21**, 104–111.
- Gust AA, Pruitt R, Nürnberg T. 2017. Sensing danger: key to activating plant immunity. *Trends in Plant Science* **22**, 779–791.
- Hacquard S, Petre B, Frey P, Hecker A, Rouhier N, Duplessis S. 2011. The poplar–poplar rust interaction: insights from genomics and transcriptomics. *Journal of Pathogens* **2011**, 716041.
- Han Z, Xiong D, Schneiter R, Tian C. 2023. The function of plant PR1 and other members of the CAP protein superfamily in plant–pathogen interactions. *Molecular Plant Pathology* **24**, 651–668.
- Haney EF, Straus SK, Hancock REW. 2019. Reassessing the host defense peptide landscape. *Frontiers in Chemistry* **7**, 43.
- Hilchie AL, Wuerth K, Hancock REW. 2013. Immune modulation by multifaceted cationic host defense (antimicrobial) peptides. *Nature Chemical Biology* **9**, 761–768.
- Hou S, Liu D, Huang S, et al. 2021. The *Arabidopsis* MIK2 receptor elicits immunity by sensing a conserved signature from phytocytokines and microbes. *Nature Communications* **12**, 5494.
- Jansson S, Douglas CJ. 2007. *Populus*: a model system for plant biology. *Annual Review of Plant Biology* **58**, 435–458.
- Jay F, Brioudes F, Voinnet O. 2023. A contemporary reassessment of the enhanced transient expression system based on the tombusviral silencing suppressor protein P19. *The Plant Journal* **113**, 186–204.
- Kohler A, Rinaldi C, Duplessis S, Baucher M, Geelen D, Duchaussoy F, Meyers BC, Boerjan W, Martin F. 2008. Genome-wide identification of NBS resistance genes in *Populus trichocarpa*. *Plant Molecular Biology* **66**, 619–636.
- Liebrand TWH, Van Den Berg GCM, Zhang Z, et al. 2013. Receptor-like kinase SOBIR1/EVR interacts with receptor-like proteins in plant immunity against fungal infection. *Proceedings of the National Academy of Sciences, USA* **110**, 10010–10015.

- Liebrand TWH, van den Burg HA, Joosten MHAJ.** 2014. Two for all: receptor-associated kinases SOBIR1 and BAK1. *Trends in Plant Science* **19**, 123–132.
- Liu H, Shen J, Yuan C, Lu D, Acharya BR, Wang M, Chen D, Zhang W.** 2021. The cyclophilin ROC3 regulates ABA-induced stomatal closure and the drought stress response of *Arabidopsis thaliana*. *Frontiers in Plant Science* **12**, 668792.
- Liu X, Wang Z, Wang W, Huang Q, Zeng Y, Jin Y, Li H, Du S, Zhang J.** 2022. Origin and evolutionary history of *Populus* (Salicaceae): further insights based on time divergence and biogeographic analysis. *Frontiers in Plant Science* **13**, 1031087.
- Lorrain C, Petre B, Duplessis S.** 2018. Show me the way: rust effector targets in heterologous plant systems. *Current Opinion in Microbiology* **46**, 19–25.
- Lu S, Faris JD, Sherwood R, Friesen TL, Edwards MC.** 2014. A dimeric PR-1-type pathogenesis-related protein interacts with ToxA and potentially mediates ToxA-induced necrosis in sensitive wheat. *Molecular Plant Pathology* **15**, 650–663.
- Marks RA, Amézquita EJ, Percivale S, Alejandra R-C, Claudia ChibiciRevneanuh SMT, Farrant JM, Chitwooda DH, VanBurenar R.** 2023. A critical analysis of plant science literature reveals ongoing inequities. *Proceedings of the National Academy of Sciences, USA* **120**, e2217564120.
- Matsushima N, Miyashita H.** 2012. Leucine-rich repeat (LRR) domains containing intervening motifs in plants. *Biomolecules* **2**, 288–311.
- Neukermans J, Inzé A, Mathys J, De Coninck B, van de Cotte B, Cammue BPA, Van Breusegem F.** 2015. ARACINs, brassicaceae-specific peptides exhibiting antifungal activities against necrotrophic pathogens in *Arabidopsis*. *Plant Physiology* **167**, 1017–1029.
- Ngou BPM, Ding P, Jones JDG.** 2022. Thirty years of resistance: zig-zag through the plant immune system. *The Plant Cell* **34**, 1447–1478.
- Nideman T, Genetet I, Bruyère T, Gees R, Stintzi A, Legrand M, Fritig B, Mössinger E.** 1995. Pathogenesis-related PR-1 proteins are antifungal. Isolation and characterization of three 14-kilodalton proteins of tomato and of a basic PR-1 of tobacco with inhibitory activity against *Phytophthora infestans*. *Plant Physiology* **108**, 17–27.
- Petre B.** 2020. Toward the discovery of host-defense peptides in plants. *Frontiers in Immunology* **11**, 1825.
- Petre B, Contreras MP, Bozkurt TO, et al.** 2021. Host-interactor screens of *Phytophthora infestans* RXLR proteins reveal vesicle trafficking as a major effector-targeted process. *The Plant Cell* **33**, 1447–1471.
- Petre B, Hacquard S, Duplessis S, Rouhier N.** 2014. Genome analysis of poplar LRR-RLP gene clusters reveals RISP, a defense-related gene coding a candidate endogenous peptide elicitor. *Frontiers in Plant Science* **5**, 111.
- Petre B, Hecker A, Germain H, Tsan P, Sklenar J, Pelletier G, Séguin A, Duplessis S, Rouhier N.** 2016. The poplar rust-induced secreted protein (RISP) inhibits the growth of the leaf rust pathogen *Melampsora larici-populina* and triggers cell culture alkalinisation. *Frontiers in Plant Science* **7**, 97.
- Petre B, Win J, Menke FLH, Kamoun S.** 2017. Protein–protein interaction assays with effector–GFP fusions in *Nicotiana benthamiana*. *Methods in Molecular Biology* **1659**, 85–98.
- Ramilowski JA, Goldberg T, Harshbarger J, et al.** 2015. A draft network of ligand–receptor-mediated multicellular signalling in human. *Nature Communications* **6**, 7866.
- Ranf S.** 2017. Sensing of molecular patterns through cell surface immune receptors. *Current Opinion in Plant Biology* **38**, 68–77.
- Rhodes J, Yang H, Moussu S, Boutrot F, Santiago J, Zipfel C.** 2021. Perception of a divergent family of phytocytokines by the *Arabidopsis* receptor kinase MIK2. *Nature Communications* **12**, 705.
- Rinaldi C, Kohler A, Frey P, et al.** 2007. Transcript profiling of poplar leaves upon infection with compatible and incompatible strains of the foliar rust *Melampsora larici-populina*. *Plant Physiology* **144**, 347–366.
- Rzemieniewski J, Stegmann M.** 2022. Regulation of pattern-triggered immunity and growth by phytocytokines. *Current Opinion in Plant Biology* **68**, 102230.
- Siepe DH, Henneberg LT, Wilson SC, Hess GT, Bassik MC, Zinn K, Christopher Garcia K.** 2022. Identification of orphan ligand–receptor relationships using a cell-based CRISPRa enrichment screening platform. *eLife* **11**, e81398.
- Snoeck S, Garcia AGK, Steinbrenner AD.** 2023. Plant receptor-like proteins (RLPs): structural features enabling versatile immune recognition. *Physiological and Molecular Plant Pathology* **125**, 102004.
- Steinbrenner AD, Munoz-Amatriain M, Chaparro AF, et al.** 2020. A receptor-like protein mediates plant immune responses to herbivore-associated molecular patterns. *Proceedings of the National Academy of Sciences, USA* **117**, 31510–31518.
- Sun Y, Chan J, Bose K, Tam C.** 2023. Simultaneous control of infection and inflammation with keratin-derived antibacterial peptides targeting TLRs and co-receptors. *Science Translational Medicine* **15**, eade2909.
- Sun Y, Wang Y, Zhang X, et al.** 2022. Plant receptor-like protein activation by a microbial glycoside hydrolase. *Nature* **610**, 335–342.
- Sung YC, Outram MA, Breen S, Wang C, Dagvadorj B, Winterberg B, Kobe B, Williams SJ, Solomon PS.** 2021. PR1-mediated defence via C-terminal peptide release is targeted by a fungal pathogen effector. *New Phytologist* **229**, 3467–3480.
- Tavormina P, De Coninck B, Nikonorova N, De Smet I, Cammuae BPA.** 2015. The plant peptidome: an expanding repertoire of structural features and biological functions. *The Plant Cell* **27**, 2095–2118.
- Thor K, Jiang S, Michard E, et al.** 2020. The calcium-permeable channel OSCA1.3 regulates plant stomatal immunity. *Nature* **585**, 569–573.
- Trifinopoulos J, Nguyen LT, von Haeseler A, Minh BQ.** 2016. W-IQ-TREE: a fast online phylogenetic tool for maximum likelihood analysis. *Nucleic Acids Research* **44**, W232–W235.
- Tuskan GA, DiFazio S, Grigoriev I, Hellsten U, Putnam NA, Ralph S.** 2006. The genome of black cottonwood, *Populus trichocarpa* (Torr. & Gray). *Science* **313**, 1596–1604.
- Ullah C, Schmidt A, Reichelt M, Tsai CJ, Gershenson J.** 2022. Lack of antagonism between salicylic acid and jasmonate signalling pathways in poplar. *New Phytologist* **235**, 701–717.
- Weber E, Engler C, Gruetzner R, Werner S, Marillonnet S.** 2011. A modular cloning system for standardized assembly of multigene constructs. *PLoS One* **6**, e16765.
- Yamaguchi Y, Huffaker A.** 2011. Endogenous peptide elicitors in higher plants. *Current Opinion in Plant Biology* **14**, 351–357.
- Yeung ATY, Gellatly SL, Hancock REW.** 2011. Multifunctional cationic host defence peptides and their clinical applications. *Cellular and Molecular Life Sciences* **68**, 2161–2176.
- Yu Z, Xu Y, Zhu L, et al.** 2020. The Brassicaceae-specific secreted peptides, STMPs, function in plant growth and pathogen defense. *Journal of Integrative Plant Biology* **62**, 403–420.
- Zhang J, Zhao J, Yang Y, Bao Q, Li Y, Wang H, Hou S.** 2022. EWR1 as a SCOPP peptide activates MIK2-dependent immunity in *Arabidopsis*. *Journal of Plant Interactions* **17**, 562–568.